NATIONAL ADVISORY COMMITTEE FOR AERONAUTICS

TECHNICAL MEMORANDUM

No. 1077

CALCULATION OF CENTRALLY LOADED THIN-WALLED COLUMNS ABOVE THE BUCKLING LIMIT

By F. Reinitzhuber

Luftfahrtforschung
Vol. 19 No. 7, July 20, 1942
Verlag von R. Oldenbourg, München und Berlin

Washington
April 1945

NATIONAL ADVISORY COMMITTEE FOR AERONAUTICS

TECHNICAL MEMORANDUM NO. 1077

CALCULATION OF CENTRALLY LOADED THIN-WALLED COLUMNS ABOVE THE BUCKLING LIMIT*

By F. Reinitzhuber

INTRODUCTION

When thin-walled columns formed from flanged sheet, such as used in airplane construction, are subjected to axial load, their behavior at failure varies according to the slenderness ratio.

On long columns the axis deflects laterally while the cross section form is maintained; buckling results. The respective breaking load in the elastic range is computed by Euler's formula and for the plastic range by the Engesser-Karman formula. Its magnitude is essentially dependent upon the length. On intermediate length columns, especially where open sections are concerned, the cross section is distorted while the cross section form is preserved; twisting failure results. The buckling load in twisting is calculated according to Wagner and Kappus (reference 1). On short columns the straight walls of low-bending resistance that form the column are deflected at the same time that the cross section form changes - buckling occurs without immediate failure. Then the buckling load of the total section computable from the buckling loads of the section walls is not the ultimate load; quite often, especially on thin-walled sections, it lies considerably higher and is secured by tests. Both loads, the buckling and the ultimate load are only in a small measure dependent upon length.

The present report is an attempt to theoretically investigate the behavior of such short, thin-walled columns above the buckling load with the conventional calculating methods.

---

*"Beitrag zur Berechnung gedrückter, dünnwandiger Profile oberhalb der Beulgrenze," Luftfahrtforschung, vol. 19, no. 7, July 20, 1942, pp. 240-247.

The cross section of the column selected was a square, which by reason of its symmetrical properties lends itself best to mathematical treatment. The results are then checked by tests.

THEORY

A closed section (hollow cylinder) of elastic material (modulus of elasticity E, Poisson's ratio ν) the cross section of which is a square with sides of length l and sheet thickness s, is centrally loaded with a force P in longitudinal direction (direction of cylinder axis). On placing through the median plane of one of the four identical sides a system of coordinates x, y, z (fig. 1), the deformations u, v, w are in direction of the coordinates, and the stresses σ_x, σ_y, and τ along the median plane.

If the mean compressive stress $p = P/4sb$ is lower than the critical buckling stress p^* the stresses are $\sigma_x = -p$, $\sigma_y = 0$, $\tau = 0$ and the deformations $u = -\frac{p}{E}x$, $v = +\nu\frac{p}{E}y$, $w = +\nu\frac{p}{E}\frac{b}{2}$. Between the shortening ϵ and the compressive stress p proportionality exists then according to the equation $p = E\epsilon$ as far as the buckling limit; at the latter $p^* = E\epsilon^*$, where ϵ^* is the critical compression.

If the mean compressive stress p exceeds the critical buckling stress p^*, the side walls wrinkle lengthwise, the cross section assumes the form shown in figure 1, on which, since the right angles remain at the corners, a bulge in the one side area corresponds to a dent in the next one and the corners remain square. If the short column is of sufficient length, the buckles in longitudinal direction have in the area not affected by the disturbed end surfaces, the constant length l; for great length, $l = b$. The behavior of the profile is therefore periodic with the length l. The problem thus reduces to an analysis of one of the four identical rectangular sides between two successive junction lines as a plate (dimensions $b \times l$).

According to the theory of the thin elastic plate with great deflections (reference 2) the stresses σ_x, σ_y, and τ in the plane of the plate follow the equations

$$\left.\begin{aligned} \frac{\partial \sigma_x}{\partial x} + \frac{\partial \tau}{\partial y} &= 0 \\ \frac{\partial \tau}{\partial x} + \frac{\partial \sigma_y}{\partial y} &= 0 \end{aligned}\right\} \tag{1a}$$

which are satisfied by the stress function formula

$$\sigma_x = \Phi_{yy},\ \sigma_y = \Phi_{xx},\ \tau = -\Phi_{xy} \tag{1b}$$

the stress function Φ and the sag w being related through the fundamental equations

$$\Delta\Delta\Phi = E\left(w_{xy}^2 - w_{xx}\, w_{yy}\right) \tag{2}$$

and

$$\frac{E s^2}{12(1-\nu^2)}\Delta\Delta w - \Phi_{yy}\, w_{xx} - \Phi_{xx}\, w_{yy} + 2\,\Phi_{xy}\, w_{xy} = 0 \tag{3}$$

The deformations u, v in the plane of the plate follow from

$$E\, u_x = \Phi_{yy} - \nu\Phi_{xx} - \frac{E}{2} w_x^2 \tag{4}$$

$$E\, v_y = \Phi_{xx} - \nu\Phi_{yy} - \frac{E}{2} w_y^2 \tag{5}$$

(The subscripts u, v, w, and Φ denote the partial derivatives conformable to the respective variables.)

The combined action between the four side walls at the corners $y = \pm b/2$ stipulates the compliance with the boundary conditions

$$w_y\left(x, \pm\frac{b}{2}\right) = -\, w_y\left(x \pm l, \pm\frac{b}{2}\right) \tag{6a}$$

$$w\left(x, \pm\frac{b}{2}\right) = v\left(x, \pm\frac{b}{2}\right) \tag{6b}$$

$$\sigma_y\left(x, \pm\frac{b}{2}\right) = 0 \tag{6c}$$

$$\tau\left(x, \pm \frac{b}{2}\right) = 0 \qquad (6d)$$

$$s \int_{-b/2}^{+b/2} \sigma_x d_y = - pbs = - \frac{P}{4} \qquad (6e)$$

Since no exact integration of equations (2) and (3) has been published so far, recourse is had to an approximate method by Maguerre (reference 2) and the Ritz formula

$$w = \eta + f \cos \frac{\pi x}{l} \cos \frac{\pi y}{b} \qquad (7)$$

is chosen for the deflection, with f as the free value which closely approaches the form of buckling occurring shortly after exceeding the critical load and satisfies (6a). Equation (7) entered at the right-hand side of equation (2) gives

$$\Delta\Delta\Phi = - \frac{E\pi^4 f^2}{2b^2 l^2} \left(\cos \frac{2\pi x}{l} + \cos \frac{2\pi y}{b}\right)$$

of which the particular integral

$$\Phi^{(p)} = - E \frac{f^2}{32} \left[\left(\frac{l}{b}\right)^2 \cos \frac{2\pi x}{l} + \left(\frac{b}{l}\right)^2 \cos \frac{2\pi y}{b}\right] \qquad (8a)$$

can be posted. For compliance with (6b) to (6d) solutions periodic in x direction and symmetrical with respect to the x and y axis

$$\Phi^{(h)} = -\left(\frac{p y^2}{2} + A \operatorname{Cosh} \frac{2\pi y}{l} \cos \frac{2\pi x}{l} + B \frac{2\pi y}{l} \operatorname{Sinh} \frac{2\pi y}{l} \cos \frac{2\pi x}{l}\right) \qquad (8b)$$

are added to the homogeneous equation $\Delta\Delta\Phi = 0$ related to (2), after which the complete solution for Φ reads

$$\Phi = \Phi^{(p)} + \Phi^{(h)} \tag{8}$$

Equation (8) for Φ entered in (1b), (4), and (5) gives

$$\sigma_x = E\frac{\pi^2}{8}\left(\frac{f}{l}\right)^2 \cos\frac{2\pi y}{b} - \frac{4\pi^2}{l^2}\cos\frac{2\pi x}{l}\left[(A + 2B)\operatorname{Cosh}\frac{2\pi y}{l} + B\frac{2\pi y}{l}\operatorname{Sinh}\frac{2\pi y}{l}\right] - p \quad \ldots(9a)$$

$$\sigma_y = \left[E\frac{\pi^2}{8}\left(\frac{f}{b}\right)^2 + \frac{4\pi^2}{l^2}\left(A\operatorname{Cosh}\frac{2\pi y}{l} + \frac{2\pi y}{l}B\operatorname{Sinh}\frac{2\pi y}{l}\right)\right]\cos\frac{2\pi x}{l} \tag{9b}$$

$$\tau = -\frac{4\pi^2}{l^2}\left[(A + B)\operatorname{Sinh}\frac{2\pi y}{l} + B\frac{2\pi y}{l}\operatorname{Cosh}\frac{2\pi y}{l}\right]\sin\frac{2\pi x}{l} \quad \ldots(9c)$$

$$Eu = -\nu E\frac{\pi^2}{8}\left(\frac{f}{b}\right)^2\frac{l}{2\pi}\sin\frac{2\pi x}{l} - E\frac{\pi^2}{8}\left(\frac{f}{l}\right)^2\left(x - \frac{l}{2\pi}\sin\frac{2\pi x}{l} - \frac{l}{2\pi}\sin\frac{2\pi x}{l}\cos\frac{2\pi y}{b}\right) - \frac{2\pi}{l}\left[(A(1 + \nu) + 2B)\operatorname{Cosh}\frac{2\pi y}{l} + (1 + \nu)B\frac{2\pi y}{l}\operatorname{Sinh}\frac{2\pi y}{l}\right]\sin\frac{2\pi x}{l} - px \tag{9d}$$

$$Ev = -\nu E\frac{\pi^2}{8}\left(\frac{f}{l}\right)^2\frac{b}{2\pi}\sin\frac{2\pi y}{b} - E\frac{\pi^2}{8}\left(\frac{f}{l}\right)^2\left(y - \frac{b}{2\pi}\sin\frac{2\pi y}{b}\frac{b}{2\pi}\cos\frac{2\pi x}{l}\sin\frac{2\pi y}{b}\right) + \frac{2\pi}{l}\left[(A(1 + \nu) - B(1 - \nu)\operatorname{Sinh}\frac{2\pi y}{l} + (1 + \nu)B\frac{2\pi y}{l}\operatorname{Cosh}\frac{2\pi y}{l}\right]\cos\frac{2\pi x}{l} + \nu py \tag{9e}$$

The boundary condition (6a) is satisfied by (7); to satisfy (6b), which with (7) becomes

$$v\left(x, \pm\frac{b}{2}\right) = \eta \tag{6b'}$$

and also (6c), (6d), and (6e); that is, of altogether four boundary conditions, only three integration constants A, B, and p are available. A suitable choice is therefore necessary to ensure satisfactory approximate solutions.

Of the four possibilities

(6b'), (6c), (6d) ..... (10a)
(6b'), (6c), (6e) ..... (10b)
(6b'), (6d), (6c) ..... (10c)
(6c), (6d), (6e) ..... (10d)

available for predicting A, B, and p, (10a) and (10b) cancel out, because for these the longitudinal borders of the plate stipulate simultaneously the conditions $\sigma_y = 0$ in (6c) and $v = \text{constant}$ in (6b'), which can be reciprocally excluded and therefore do not eliminate the boundary integral in equation (13). With (10c) and (10d) it is found from (6e) by integration of (9a) for σ_x over the plate width by observation of (6d), that the constant of integration p is directly equal to the average value of the compressive stress

$$p = \frac{P}{4bs} \qquad (11a)$$

The other two unknown constants A and B are then obtained conformably to (10c) and (10d) from (6b), (6d) or (6c) and (6d). From (6b) and (6d) the result is $A = B = 0$; this case, already investigated by Marguerre on the effective width of the stiffened plate in compression (reference 2), is not as suitable an approximate solution as those obtainable from (6c) and (6d) and which were therefore used for computing A and B.

Equations (9b) and (9c) afford for $y = \pm b/2$ in accord with (6c) and (6d) the equations

$$A\left(\frac{2\pi}{l}\right)^2 \operatorname{Cosh} \pi \frac{b}{l} + B\left(\frac{2\pi}{l}\right)^2 \pi \frac{b}{l} \operatorname{Sinh} \pi \frac{b}{l} + E \frac{\pi^2}{8}\left(\frac{f}{b}\right)^2 = 0$$

$$A \operatorname{Sinh} \pi \frac{b}{l} + B\left(\operatorname{Sinh} \pi \frac{b}{l} + \pi \frac{b}{l} \operatorname{Cosh} \pi \frac{b}{l}\right) = 0$$

hence

$$A = -\frac{Ef^2}{16}\left(\frac{l}{b}\right)^2 \frac{\operatorname{Sinh}\pi\frac{b}{l} + \pi\frac{b}{l}\operatorname{Cosh}\pi\frac{b}{l}}{\operatorname{Sinh} 2\pi\frac{b}{l} + 2\pi\frac{b}{l}} \qquad (11b)$$

$$B = +\frac{Ef^2}{16}\left(\frac{l}{b}\right)^2 \frac{\operatorname{Sinh}\pi\frac{b}{l}}{\operatorname{Sinh} 2\pi\frac{b}{l} + 2\pi\frac{b}{l}} \qquad (11c)$$

The constants of integration A, B, and p given by (11) satisfy (10d) but not (6b') which specifies that the deformation v on the longitudinal edge of the plate shall be constant and equal to η, and for which (9e) gives

$$v\left(x, \pm\frac{b}{2}\right) = \left(-\frac{\pi^2}{8}\left(\frac{f}{b}\right)^2 + \nu\frac{p}{E}\right)\frac{b}{2} + \frac{2\pi}{lE}\left\{[A(1+\nu) - B(1-\nu)]\operatorname{Sinh}\pi\frac{b}{l} + (1+\nu)B\pi\frac{b}{l}\operatorname{Cosh}\pi\frac{b}{l}\right\}\cos\frac{2\pi x}{l}$$

On posting herein the values (11b) and (11c) for A and B it is found that in fact the second summand variable with x does not disappear, hence that $v(x, \pm b/2)$ does not become constant. In order to obtain a value for η independent of x with the least possible deviations from (6b')

$$\eta = \left(-\frac{\pi^2}{8}\left(\frac{f}{b}\right)^2 + \nu\frac{p}{E}\right)\frac{b}{2}$$

is put equal to the average value of v at the longitudinal plate edge.

The equation (3) for w can no longer be satisfied, in consequence of Ritz's formula and is therefore replaced by the demand to so choose the free value f that the form change energy stored in the plate

$$\bar{A} = \int_{-l/2-b/2}^{+l/2+b/2}\int \left\{\frac{s}{2E}[(\Delta\Phi)^2 - 2(1+\nu)(\Phi_{xx}\Phi_{yy} - \Phi_{xy}^2)] + \frac{Es^3}{24(1-\nu^2)}[(\Delta w)^2 - 2(1-\nu)(w_{xx}w_{yy} - w_{xy}^2)]\right\}dx\,dy \qquad (12)$$

becomes a minimum. The unknown f is determined from $\frac{\partial \bar{A}}{\partial f} = 0$. Differentiation of (12) with respect to f before integrating (Galerkin method), while bearing in mind (1a) instead of (3) gives

$$\frac{\partial \bar{A}}{\partial f} = -s \int_{-l/2}^{+l/2} \int_{-b/2}^{+b/2} \left(\Phi_{yy} w_{xx} + \Phi_{xx} w_{yy} - 2 \Phi_{xy} w_{xy} - \frac{E s^2}{12(1-\nu^2)} \Delta\Delta w \right) \frac{\partial w}{\partial f} \, dx \, dy$$

$$+ s \int_{-b/2}^{+b/2} \left| \left[\Phi_{yy} \left(\frac{\partial u}{\partial f} + w_x \frac{\partial w}{\partial f} \right) - \Phi_{xy} \left(\frac{\partial v}{\partial f} + w_y \frac{\partial w}{\partial f} \right) \right] \right|_{x = \pm l/2} dy$$

$$+ s \int_{-l/2}^{+l/2} \left| \left[\Phi_{xx} \left(\frac{\partial v}{\partial f} + w_y \frac{\partial w}{\partial f} \right) - \Phi_{xy} \left(\frac{\partial u}{\partial f} + w_x \frac{\partial w}{\partial f} \right) \right] \right|_{y = \pm b/2} dx$$

$$+ \frac{E s^3}{12(1-\nu^2)} \left\{ \int_{-b/2}^{+b/2} \left| (\nu w_{xyy} - 2 w_{xyy} - w_{xxx}) \frac{\partial w}{\partial f} \right|_{x = \pm l/2} dy \right.$$

$$+ \int_{-l/2}^{+l/2} \left| (\nu w_{xxy} - 2 w_{xxy} - w_{yyy}) \frac{dw}{\partial f} \right|_{y = \pm b/2} dx$$

$$+ \int_{-b/2}^{+b/2} \left| (w_{xx} + \nu w_{yy}) \frac{\partial w_x}{\partial f} \right|_{x = \pm l/2} dy + \int_{-l/2}^{+l/2} \left| (w_{yy} + \nu w_{xx}) \frac{\partial w_y}{\partial f} \right|_{y = \pm b/2} dx$$

$$\left. + 2(1-\nu) \left| w_{xy} \frac{\partial w}{\partial f} \right| \right\} = 0 \qquad (13)$$

$$x = \pm l/2$$

$$y = \pm b/2$$

In equation (13) the boundary terms and integrals disappear with formula (7) and the boundary conditions (6c) and (6d).

With the solution of f from (13) the stress and strain condition of the section can be calculated from equations (7) and (9).

The subsequent investigation is carried out for the case of square bulges ($b = l$), as they occur in the undisturbed zone on the sufficiently long cylinder. Entering the expression (8) for Φ and (11) for A and B, equation (11) yields

$$\epsilon - \frac{\pi^2}{3}\left(\frac{s}{l}\right)^2 \frac{1}{1-\nu^2} - \frac{\pi^2}{8}\left(\frac{f}{l}\right)^2(2-\kappa) = 0 \qquad (14)$$

where p is replaced by the expression

$$p = E\left(\epsilon - \frac{\pi^2}{8}\left(\frac{f}{l}\right)^2\right) \qquad (15)$$

following from $u\left(\pm\frac{l}{2}, y\right) = \pm\epsilon\frac{l}{2}$ (cf. equation (9d)) and

$$\kappa = \frac{\text{Cosh } 2\pi - 1}{\pi(2\pi + \text{Sinh } 2\pi)} = 0.30985$$

Posting $f = 0$ in (14) gives the critical value for the shortening ϵ:

$$\epsilon(f = 0) = \frac{\pi^2}{3}\left(\frac{s}{l}\right)^2 \frac{1}{1-\nu^2} = \epsilon^*$$

hence (14) gives

$$\frac{\pi^2}{8}\left(\frac{f}{l}\right)^2 = k(\epsilon - \epsilon^*) \quad \left(k = \frac{1}{2-\kappa} = 0.5917\right) \qquad (16)$$

The connection between mean stress p and mean ϵ follows from (15) with

$$p - p^* = E_{red}(\epsilon - \epsilon^*) \qquad (17)$$

where

$$E_{red} = (1 - k)\, E = \frac{1 - \kappa}{2 - \kappa}\, E = 0.4083\, E$$

The stress–strain equation (17) is reproduced in figure 2. The apparent stiffness above the buckling limit is thus only about 0.4 times as great as below the critical buckling load.

Entering (16) and (17) in (7) and (9) gives

$$\frac{\sigma_x}{p^*} = -\frac{p}{p^*} + \frac{1}{1-\kappa}\left(\frac{p}{p^*} - 1\right)\left\{\cos\frac{2\pi y}{l} - \cos\frac{2\pi x}{l}\left[(\alpha + 2\beta)\operatorname{Cosh}\frac{2\pi y}{l} + \beta\frac{2\pi y}{l}\operatorname{Sinh}\frac{2\pi y}{l}\right]\right\}$$

$$\frac{\sigma_y}{p^*} = \frac{1}{1-\kappa}\left(\frac{p}{p^*} - 1\right)\cos\frac{2\pi x}{l}\left\{1 + \alpha\operatorname{Cosh}\frac{2\pi y}{l} + \beta\frac{2\pi y}{l}\operatorname{Sinh}\frac{2\pi y}{l}\right\}$$

$$\frac{\tau}{p^*} = \frac{1}{1-\kappa}\left(\frac{p}{p^*} - 1\right)\sin\frac{2\pi x}{l}\left\{(\alpha + \beta)\operatorname{Sinh}\frac{2\pi y}{l} + \beta\frac{2\pi y}{l}\operatorname{Cosh}\frac{2\pi y}{l}\right\}$$

$$\left(\alpha = -0.35008,\ \beta = +0.08429,\ \frac{1}{1-\kappa} = 1.44896\right)$$

The numerical evaluation of these equations for simple exceeding of the buckling load $(p/p^* = 2)$ is shown in figure 3.

The stress distribution gives only an approximate picture of the actual condition, because the deformation of v at the section edge is not constant and independent of x as (6b') stipulates. In spite of that the stress distribution is quite plain: the wavelike deflections in the side walls after the critical buckling load is exceeded tend to pull the corners into the area of maximum deflections. This results in tensile stresses in y direction in the middle of the buckles which balance the compressive stresses occurring in the reversal

point of the waves. This balance can be established only with the aid of shearing stresses. The compressive stresses in x direction are unevenly distributed after the critical buckling load is exceeded, the compressive stresses move toward the corners. Depending upon the position of the cross section the shearing stresses produce a different type of stress distribution over the plate width so that the shift of the compressive stress on the plate edges is greater in the cross section with maximum deflection than in the cross section at the reversal point of the waves.

The reason that the investigation carried out in the foregoing is only approximately valid lies in the form of buckle established with formula (7) for which the corners were assumed to be square. With increasing exceeding of the critical buckling load the corners of the section cease to remain square, but pull into the cross sections in which the side walls are subjected to the greatest deformations. An extension of formula (7) by addition of a second free value of the type

$$w = \eta + f_1 \cos \frac{\pi x}{l} \cos \frac{\pi y}{b} + f_2 \cos \frac{2\pi x}{l} \cos \frac{2\pi y}{b}$$

and further terms of this series should certainly produce better results. If it is desired to use only one free value and to achieve an improvement, formula (7) might be retained and other solutions of the homogeneous equation $\Delta\Delta\Phi = 0$ with new constants of integration added in (8b) and these then determined by point-by-point compliance with the boundary conditions. However, the paper work involved is so great that its application was foregone.

EXPERIMENT

The purpose of the tests was to check the aforementioned theoretical results by actual experiments, with special reference to formula (7) and the stress-strain formula (17).

The test specimen was a square cylinder (fig. 4) of medium hard sheet brass with the rivet seam running along the center of a side. The characteristics of the brass sheet (airplane material identification 2160.7) were:

Thickness of sheet s = 0.61 to 0.62 mm, average: 0.615 mm

Modulus of elasticity E = 10,000 to 11,000 kg/mm², average: 10,500 kg/mm²

Yield point $\sigma_{0.2}$ = 24.4 kg/mm²

Tensile strength σ_B = 35.2 to 38.6 kg/mm²

Elongation δ = 50 percent

The wrinkles were measured on two side walls by means of a dial gage and a machined angle section, with arm set parallel to two sides of the cylinder as shown in figure 4. The sides parallel to the arms were explored by shifting the dial gage. The deformations normal to the direction of compression were measured in the center of the two side walls over the entire length and at two cross sections (test station 18 and 25). The length change of the diagonals under increasing load was recorded by vernier calipers, the compression of the test specimen by dial gage. The first reading was made at 30-kilogram load; the other load stages at which measurements were made, were 200, 500, 700, 1000, and 1200 kilograms.

The results of the side wall measurements are shown in figure 5. According to figures 5a and 5b, the waves formed in longitudinal direction are approximately alike so far as the uniformity was not disturbed by pre-buckling and edge effects. An increase in load was accompanied by a slight change in the wave length. As one side area bulged out the area next to it bulged in and vice versa.

The length change of the diagonals is represented in figure 6. The absolute size of these deformations is small compared to the side wall bulging. Serviceable test values start at 1300-kilogram loading, shortly before the breaking load is reached. The points at which the waves in the side areas have their extreme values disclosed a reduction in length of the diagonals, the junction lines of the waves a slight increase in corner distance.

The result of the compression measurement on the test specimen under increasing load is given in table 1.

The specimen fails at P = 1330 kilograms through deformation of the corners at test stations 33 and 34, where the waves of the side areas have their junction lines. The failure (fig. 7) appears to be instability failure.

On the basis of the side wall measurements formula (7) can be regarded as depicting the deformation area so long as the critical load is not too greatly exceeded; if further exceeded the corners will not remain square, so that formula (7) yields inferior approximate solutions, as already indicated.

With a view to comparing the experimental data for the compression with the theoretically obtained stress-strain equation the values of table 1 were plotted in figure 2, where

$$\epsilon^* = \frac{\pi^2}{3} \frac{1}{1 - 0.3^2} \left(\frac{0.0615}{8.0} \right)^2 = 0.000213$$

$$p^* = 0.000213 \times 1050{,}000 = 224 \text{ kg/cm}^2$$

Good agreement obtains up to a simple exceeding of the critical buckling load ($p/p^* = 2$). Failure occurred at 2.3 times exceeding of the critical buckling load ($p/p^* = 3.3$). In the elastic range, before reaching the theoretical critical buckling load, the test points do not lie on the theoretical straight line, which is probably attributable to the prebuckling inevitable on thin sheet. On the basis of the good agreement of the theoretical stress-strain curve above the critical buckling load the calculation of the constants of integration A and B from (10d) appears therefore justified also. The use of (10c) as basis of the study would have resulted in a decrease of the apparent stiffness above the buckling limit by 0.5 times of the value valid in the elastic range, a result obviously less in agreement with the test data of figure 2 than that secured from (10d) with $E_{red} = 0.408\ E$ (equation 17).

A check test of the stress-strain curve was run on a specimen of duralumin with the same cross section as that of figure 4 (aircraft material 3116.5), (length: $l = 800$ m/m). Its general characteristics were as follows:

Sheet thickness $s = 0.61$ to 0.67 mm, average $= 0.64$ mm

Modulus of elasticity $E = 6540$ to 7320 kg/mm^2, average 6830 kg/mm^2

Yield limit $\sigma_{0.2} = 29.1$ kg/mm^2

Tensile strength $\sigma_B = 41.6$ to 42.2 kg/mm^2

Elongation $\delta = 20$ percent

The compression with increasing load was measured; the results are given in table 2. On putting the test values of table 2 in ratio to the critical values

$$\epsilon^* = \frac{\pi^2}{3} \frac{1}{1 - 0.3^2} \left(\frac{0.064}{8.0}\right)^2 = 0.000232$$

$$p^* = 0.000232 \times 683{,}000 = 158 \text{ kg/cm}^2$$

followed by plotting in figure 2 it is found that the theoretical stress-strain curve is here also in good agreement with the test points up to a simple exceeding of the critical buckling load. Failure occurred at P = 1350 kilograms, which corresponds to a 3.1 times exceeding of the critical buckling load.

Summing up it may be stated that the tests fulfilled their purpose, namely, to check the formula (7) and the stress-strain equation (17). As a consequence the stress-strain equation (17) secured theoretically with formula (7) can be regarded as practical up to a simple exceeding of the critical buckling load.

CONCLUDING NOTE

On the basis of the present report it is possible to obtain a picture of the stress distribution and the strain condition in a thin-walled, centrally loaded column of square cross section above the critical buckling load, as well as an insight into the relationship existing between stress and strain. Above the critical buckling load the stress-strain curve is linear according to formula (7) in first approximation for the square section just as for the stiffened plate in compression, except that the range in which this equation is applicable, is much greater compared to the breaking load than on the compressed plate. While the test specimens described previously failed at 2.3 and 3.1 times exceeding of the critical buckling load, the excess on the stiffened plate

in compression may rise to several hundred times above the critical buckling load, before the plate fails. The knowledge of the stress-strain equation is important when these sections are used as stiffeners on compressed plates. The decrease in section stiffness above the critical buckling load with the effective width must then be allowed for.

The theoretical prediction of the breaking value of thin-walled flanged sections in compression is beset with great difficulties since, apart from the obstacles indicated in the present report, difficulties arise even in the elastic range, the stress peaks in the corners exceed the elasticity limit before the breaking value is reached and the premises of the theory then do no longer hold. If, on the other hand, the obtainment of the elastic limit by the stress peaks is regarded as a measure for the load capacity of the sections, the methods applied here make it possible to obtain approximate values for the allowable loads by theoretical means.

Translation by J. Vanier,
National Advisory Committee
for Aeronautics.

REFERENCES

1. Wagner, Herbert: Torsion and Buckling of Open Sections. NACA TM No. 807, 1936.

Kappus, Robert: Twisting Failure of Centrally Loaded Open-Section Columns in the Elastic Range. NACA TM No. 851, 1938.

2. Marguerre, Karl: The Apparent Width of the Plate in Compression. NACA TM No. 833, 1937.

Kromm, A. and Marguerre, Karl: Behavior of a Plate Strip under Shear and Compressive Stresses beyond the Buckling Limit. NACA TM No. 870, 1938.

TABLE I

P (kg)	$p = \frac{P}{F}$ (kg/cm²)	Δl (mm)	$\epsilon = \frac{\Delta l}{l}$
0	0	0	0
200	102	0.05	$.58 \times 10^{-4}$
300	152	.09	1.05
400	203	.14	1.63
500	254	.22	2.56
600	305	.34	3.95
700	355	.44	5.11
800	406	.55	6.39
900	457	.67	7.79
1000	508	.80	9.30
1100	558	.92	10.69
1200	609	1.16	13.48
1300	660	1.47	17.08

TABLE 2

P (kg)	$p = \frac{P}{F}$ (kg/cm²)	Δl (mm)	$\epsilon = \frac{\Delta l}{l}$
0	0	0	0
100	49	.053	$.66 \times 10^{-4}$
200	97	.108	1.35
300	146	.175	2.19
400	195	.298	3.73
500	244	.440	5.50
600	293	.590	7.38
700	341	.780	9.75
800	390	.968	12.10
900	439	1.195	14.95
1000	488	1.433	17.90

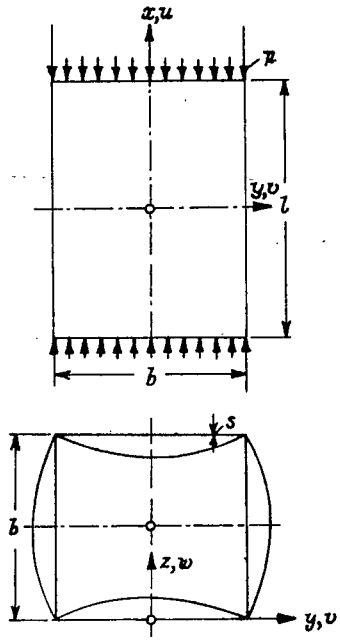

Figure 1.- Square section under uniform compression.

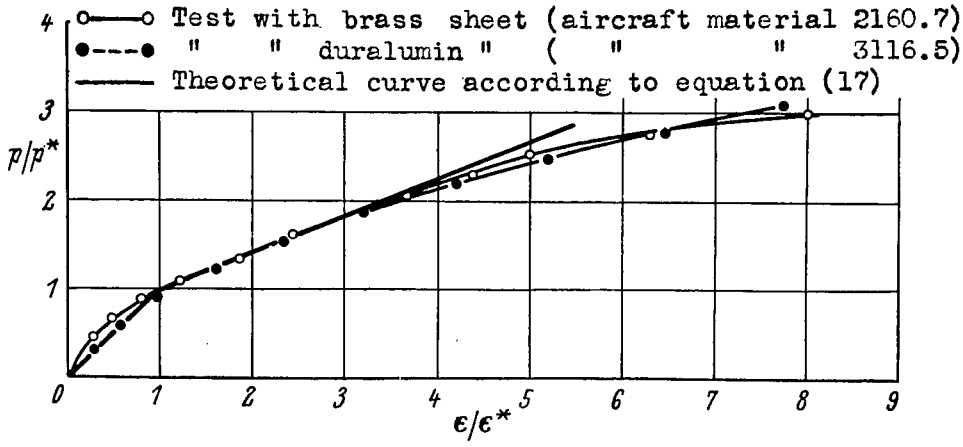

Stress strain curves

Figure 2.- $p^* = \frac{\pi^2}{3} \frac{E}{1-\nu^2} \left(\frac{S}{l}\right)^2$ critical buckling load; $\epsilon^* = \frac{p^*}{E}$ critical shortening.

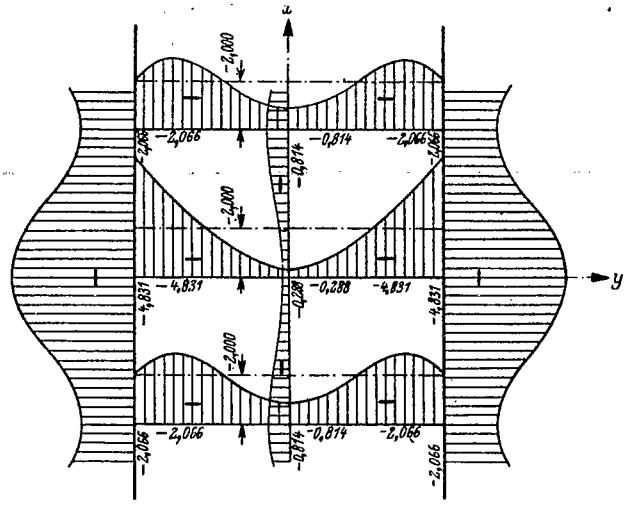

(3a) Normal stress $\frac{\sigma x}{p^*}$

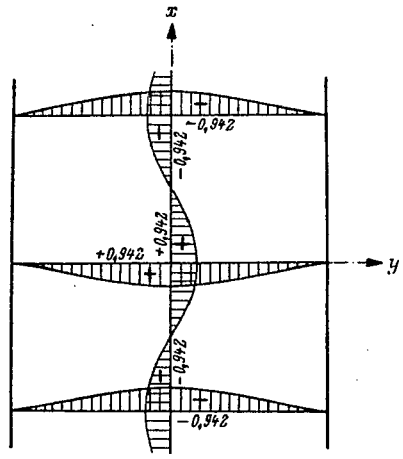

(3b) Normal stress $\frac{\sigma y}{p^*}$

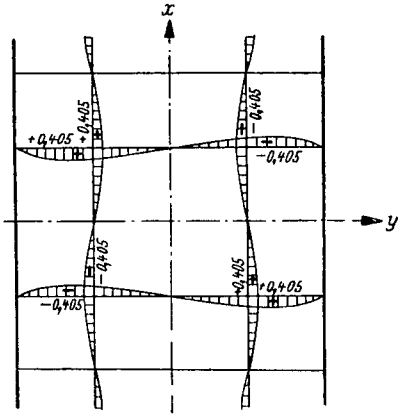

(3c) Shear stress $\frac{\tau}{p^*}$

Figures 3a to 3c.- Stress distribution in the side wall of a thin-walled centrally loaded section with square cross section above the critical buckling load $\left(\frac{p}{p^*} = 2\right)$.

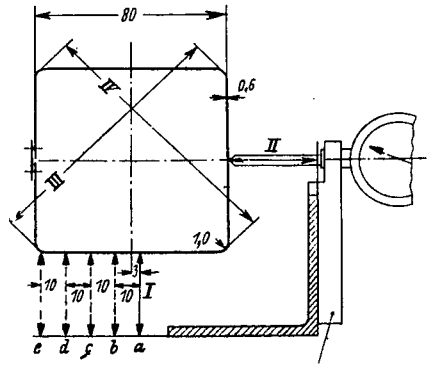

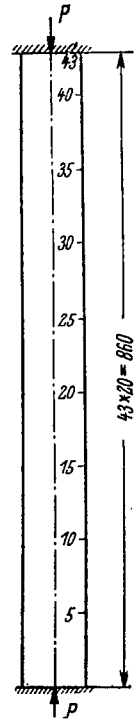

Figure 4.- Dimensions of test specimen brass sheet, (aircraft material 2160.7); dimensions in mm.

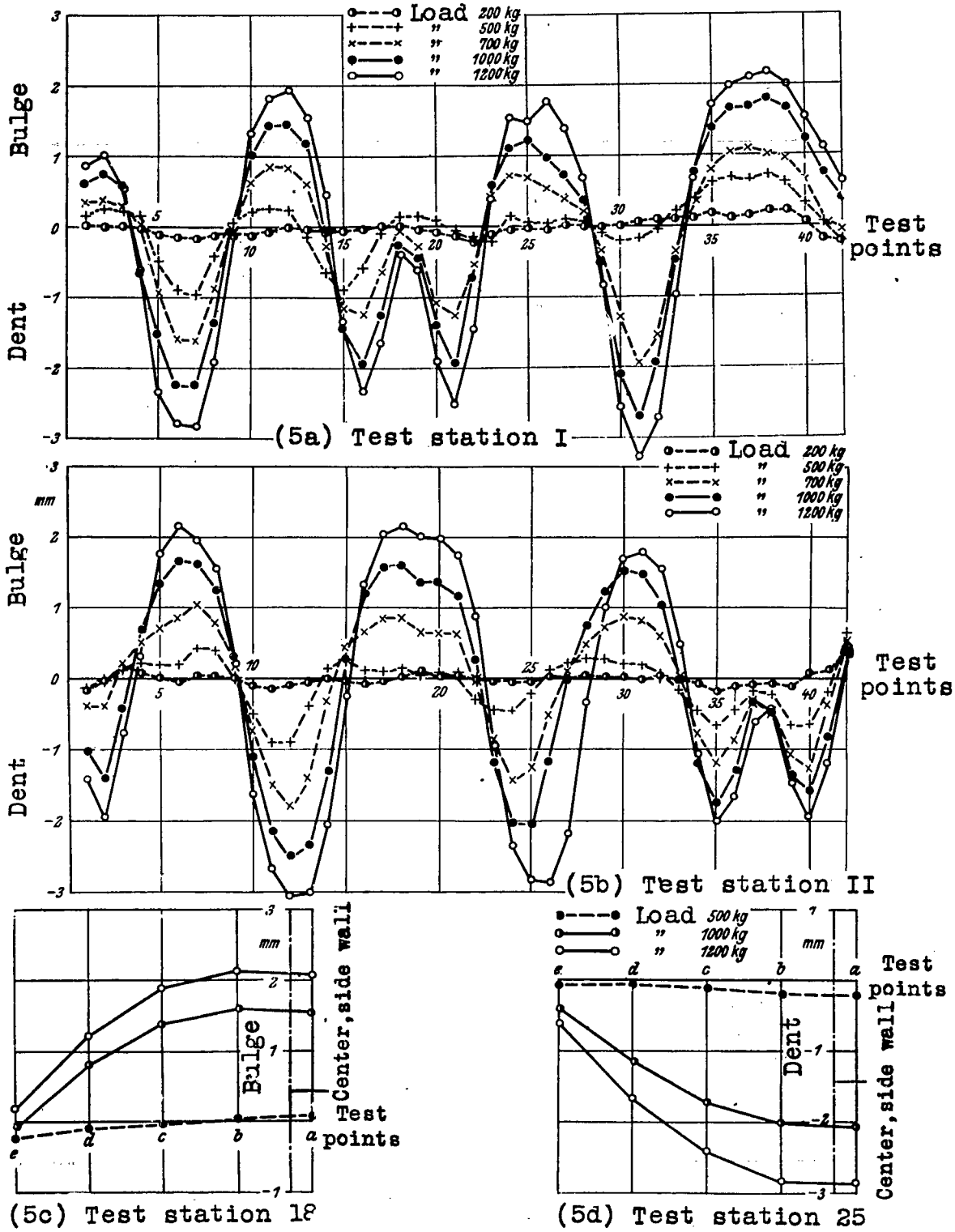

Figures 5a to 5d. Measurements on side walls of test specimen, (aircraft material 2160.7)

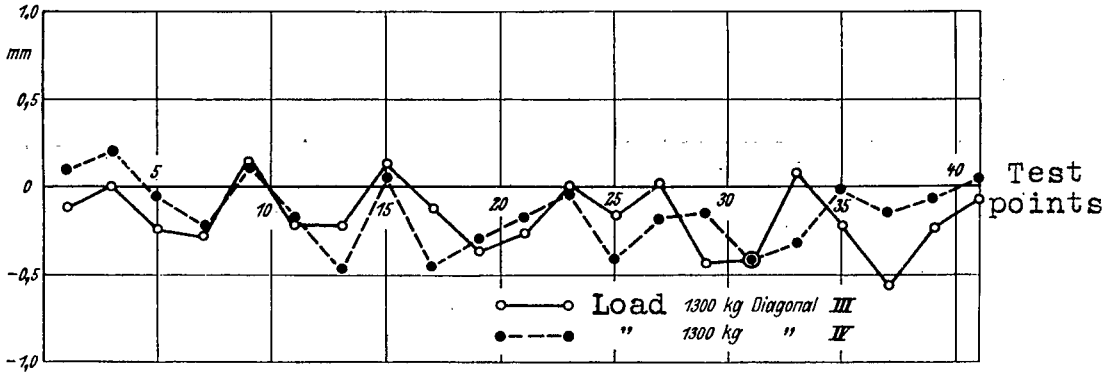

Figure 6.- Length changes in the diagonals (test stations III and IV) of the brass test specimen (aircraft material 2160.7).

Figure 7.- Specimen after test.

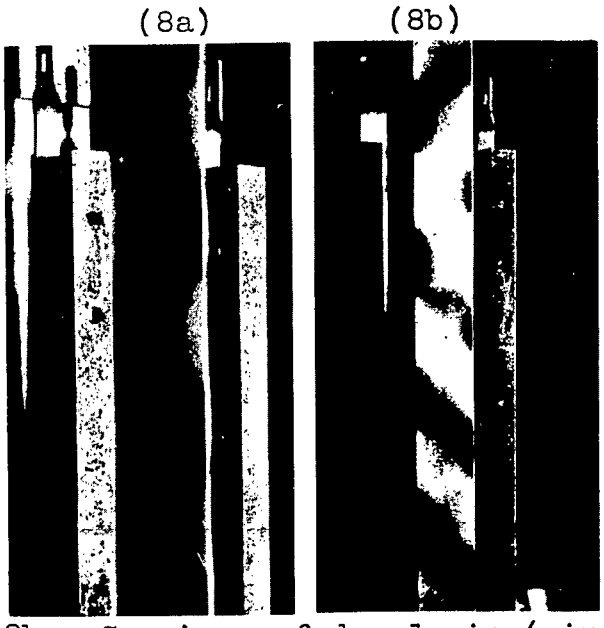

Figures 8a and 8b.- Specimen of duralumin (aircraft material 3116.5) under compressive load of 1200 kg.